Research Article Vol. 15, No. 5 / 1 May 2024 / Biomedical Optics Express 3251
Biomedical Optics EXPRESS

Analysis of age-related changes in the left ventricular myocardium with multiphoton microscopy

JUAN M. BUENO,[1,*] ROSA M. MARTÍNEZ-OJEDA,[1] MARÍA PÉREZ-ZABALZA,[2,3] LAURA GARCÍA-MENDÍVIL,[2] M. CARMEN ASENSIO,[1] LAURA ORDOVÁS,[2,4] AND ESTHER PUEYO[2,5]

[1]*Laboratorio de Óptica, Instituto Universitario de Investigación en Óptica y Nanofísica, Universidad de Murcia, Campus de Espinardo (Ed. 34), 30100 Murcia, Spain*
[2]*BSICoS group, I3A, IIS Aragón, Universidad de Zaragoza, 50018 Zaragoza, Spain*
[3]*Centro Universitario de la Defensa (CUD), 50018 Zaragoza, Spain*
[4]*Fundación Agencia Aragonesa para la Investigación y el Desarrollo (ARAID), 50018 Zaragoza, Spain*
[5]*Centro de Investigación Biomédica en Red de Bioingeniería, Biomateriales y Nanomedicina, 50018 Zaragoza, Spain*
[*]*bueno@um.es*

Abstract: Aging induces cardiac remodeling, resulting in an increase in the risk of suffering heart diseases, including heart failure. Collagen deposition increases with age and, together with sarcomeric changes in cardiomyocytes, may lead to ventricular stiffness. Multiphoton (MP) microscopy is a useful technique to visualize and detect variations in cardiac structures in a label free fashion. Here, we propose a method based on MP imaging (both two-photon excitation fluorescence (TPEF) and second harmonic generation (SHG) modalities) to explore and objectively quantify age-related structural differences in various components of cardiac tissues. Results in transmural porcine left ventricle (LV) sections reveal significant differences when comparing samples from young and old animals. Collagen and myosin SHG signals in old specimens are respectively 3.8x and >6-fold larger than in young ones. Differences in TPEF signals from cardiomyocyte were ~3x. Moreover, the increased amount of collagen in old specimens results in a more organized pattern when compared to young LV tissues. Since changes in collagen and myosin are associated with cardiac dysfunction, the technique used herein might be a useful tool to accurately predict and measure changes associated with age-related myocardium fibrosis, tissue remodeling and sarcomeric alterations, with potential implications in preventing heart disease.

1. Introduction

Cardiovascular disease (CVD) is the leading cause of death globally. It is estimated to account for nearly 17.9 million deaths yearly [1]. Age induces a number of molecular, cellular and structural changes that deteriorate the functionality of the cardiovascular system and increase the risk of CVD. From studies in animal species, it is known that aging augments the deposition of extracellular matrix (i.e. fibrosis) leading to ventricular wall stiffness, less contraction force, and thus, heart malfunctioning [2,3]. Fibrosis is also a well-known arrhythmogenic substrate as it can hamper proper impulse propagation [4]. Recently, similar observations have been reported in humans and large animals (pig) in relation to age and fibrosis (amount and spatial distribution), and specifically related to collagen as chief component of the ventricular extracellular matrix [5,6].

Maintenance of normal systolic function is also dependent on the adequate operation of the contraction machinery within cardiomyocytes. Myosin protein in combination with actin

#509227 https://doi.org/10.1364/BOE.509227
Journal © 2024 Received 12 Oct 2023; revised 27 Jan 2024; accepted 11 Mar 2024; published 23 Apr 2024

Biomedical Optics EXPRESS

filaments are the engine that transforms energy into movement. The two isoforms of myosin, Myosin Heavy Chain 7 (MYH7) and Myosin Heavy Chain 6 (MYH6), are known to be regulated in a species-specific manner during development, disease and aging [7]. The human heart is mostly formed by MYH7 and some MYH6, the latter thought to be important in maintaining normal systolic function [8,9]. Failing human hearts lack MYH6 [10,11], but whether deregulation of myosin with age occurs in humans and large animals remains unknown.

Understanding age-related alterations in collagen dynamics and changes in myosin homeostasis is fundamental to shed light on the enhanced risk of suffering heart disease with age. Novel approaches to assess the structural changes occurring at the tissue level are of special relevance to retrieve novel insight in cardiac remodeling. Ideally, methods that minimize tissue processing, to preserve its native features, and of high resolution are desirable.

Multiphoton microscopy (MP) is a versatile technique used for high-resolution deep tissue imaging without the use of exogenous stains [12]. Two different MP signals are widely used: Second Harmonic Generation (SHG) and Two Photon Excitation Fluorescence (TPEF). The former allows visualizing non-centrosymmetric structures such as type I collagen and myosin [13,14]. The latter is emitted by endogenous fluorophores (proteins, mitochondrial NAD(P)H, flavins, elastin, organelles,. . .) [15]. Since MP emission requires a high density of incident infrared photons, the signal is limited to the focal spot, which provides inherent confocality and reduced photodamage [12]. Whereas TPEF is an incoherent process which is emitted over the entire solid angle (i.e. 4π steradians), SHG emission is a coherent process, which normally favors the forward rather than the backward emission direction due to the phase matching requirement [16,17]. Despite these noticeable differences, TPEF and SHG imaging techniques have been successfully used in biomedicine to evaluate a great variety of non-labelled biological tissues, including skin, cancer-related tumors, corneas, dental pieces and brain, among others [12,15,18–22]. MP microscopy was also used to differentiate healthy from pathological tissues [22–25] and to evaluate age-related changes [26–29].

To the best of our knowledge, Rubart et al. were the first to use MP microscopy to explore cardiac structures. In particular, they used TPEF signal to monitor spontaneous and stimulation-evoked calcium transients in individual cardiomyocytes in the left ventricular myocardium of a mouse (through changes in rhod-2 indicator dye fluorescence) [30]. TPEF signal from enhanced green fluorescent protein (EGFP)-expressing donor cardiomyocytes was subsequently used to image intracellular calcium-dependent changes in the intact recipient heart [31,32]. Although MP microscopy has been extensively used to explore dynamic events (e.g., calcium transients) on a subcellular scale within cardiac tissue (see [33] as a general reference), other studies paid attention to the potential of this technique to visualize different heart regions and to explore changes under different experimental conditions. Ziptel and co-authors reported a merged MP image showing collagen scaffolding (SHG signal) surrounding a cardiac myocyte (TPEF signal from NAD(P)H)) in a freshly excised mouse heart tissue [34]. However, they did not provide any additional quantitative information. In fixed cardiomyocytes of sheep fetuses, SHG demonstrated high-contrast images of myosin filaments and TPEF clearly visualized cell morphology [35]. SHG microscopy was applied to image freshly isolated unstained myocytes from an adult frog heart with 20-nm accuracy. Given the remarkable efficiency and contrast of the images, individual sarcomere length was accurately assessed [36]. The combination of both MP signals was also employed to investigate changes in pig coronary artery wall architecture during transmural pressurization [37]. Moreover, collagen and elastin of bovine aortic heart valves were visualized by means of SHG and TPEF imaging respectively, without fixation or staining requirements [38].

Cardiac abnormalities and certain pathologies have also been explored with MP microscopy. These included infarcts, atrial fibrillation and fibrosis, among others. SHG and TPEF images from the infarct border zone of a transgenic mouse heart were acquired in a proof-of-concept experiment by Scherschel and Rubart [33]. Whereas SHG intensity arose from the collagen distribution

Biomedical Optics EXPRESS

within the infarct scar, TPEF signal was obtained exclusively in the cardiomyocytes. In the human atrial myocardium, SHG images showed differences in the morphology and the arrangement of collagen fibers between normal sinus rhythm and atrial fibrillation (i.e., arrhythmia) tissues [39]. Altered collagen deposition in diseased mouse hearts following hypertrophic remodeling [40] and structural alterations caused by pressure-overload in murine hearts [41] were verified by means of SHG signals. 3D SHG microscopy was also useful to characterize the fibrotic network in cleared cardiac muscle sections of rats [42]. Age-related morphological alterations in the marmoset heart were investigated through TPEF and SHG imaging [43]. More recently, Garcia-Mendivil and colleagues performed quantitative and spatial characterization of collagen in the left ventricle (LV) myocardium of young to old pigs, and human donors [6] to analyze its potential implications for ventricular arrhythmia development with age. Consistency between pig and human results led the authors to consider the pig as a relevant model of age-related heart changes. However, changes in myosin or other collagen structural features such as density or arrangement-related parameters, were not evaluated.

Most of these previous studies were limited to subjective descriptions and objective measurements were no reported. Therefore, it is crucial to go a step further to improve the existing procedures to accurately explore age-associated changes in LV located not only at the interstitial areas (collagen), but also within the myocardial fibers (myosin). In that sense, the aim of this work is to develop a method to objectively analyze MP signals (TPEF and SHG) in the heart tissue to gain novel insight into the age-related remodeling of collagen and myosin. Specifically, collagen density and structural arrangements, as well as variations in myosin concentration are investigated.

2. Methods

2.1. Animal tissues

Pig transmural LV tissue specimens were collected from young female pigs (N = 4, 16 weeks old) and old male pigs (N = 3, 4-5 years old), provided by the Experimental Surgery Service of the Biomedical Research Center of Aragón (CIBA, Zaragoza, Spain) and a local slaughterhouse (The Pink Pig, Zaragoza, Spain), respectively. The samples were obtained 10-15 minutes after the sacrifice with a disposable biopsy needle and processed as explained in detail in [6,44]. Routine hematoxylin-eosin staining was performed to select only tissue specimens that presented the myocardial fibers in their longitudinal axis in order to correctly visualize the SHG signal from myosin [14]. Each adjacent tissue section (5-µm in thickness) was left unstained and was mounted on a microscope slide for MP imaging.

This experiment was approved by the Ethics Committee on Animal Experimentation, (CEAEA) of the University of Zaragoza. All animal experiments followed the guidelines of the local animal welfare committee for the care and use of experimental animals and complied with the Directive 2010/63/EU of the European Parliament on the protection of animals used for scientific purposes.

2.2. Multiphoton microscope

Figure 1 shows a schematic of the home-made inverted MP microscope used for the purpose of this work [45]. The illumination source is a Ti:Sapphire femtosecond laser ($\lambda = 800$ nm, 76 MHz repetition rate, 120 fs pulses) which passes through a neutral density filter (NDF), a beam expander (BE) and a XY scanning unit (composed of two non-resonant galvanometric mirrors). The beam is then reflected by a dichroic mirror (DIC), travels through a long working-distance objective (Numerical Aperture [NA] = 0.5, 20x) and reaches the sample. The emitted signal (TPEF and/or SHG) is collected by the same objective, passes the spectral filters, finally reaching the detection system (photomultiplier tube, PMT). The spectral filters were used to isolate each

Biomedical Optics EXPRESS

MP signal: SHG (narrow band filter, 400 ± 10 nm) and TPEF (broadband filter, 435-700 nm). The experimental setup was fully controlled through a LabView software.

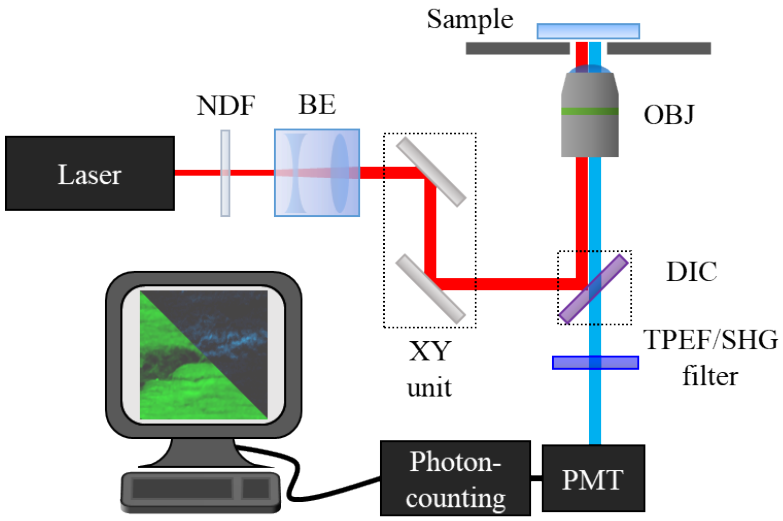

Fig. 1. Schematic representation of the MP microscope used in this work. See text for details.

2.3. *Image processing*

2.3.1. Image segmentation

For each sample, series of SHG-TPEF image pairs from different and randomly chosen locations were recorded (42 and 52 pairs in young and old hearts, respectively). In particular, two tissue structures of interest within the cardiac tissue were considered: (#1) the interstitial areas (zones corresponding to the collagen within the cardiac intercellular space) and (#2) the cardiac muscle fibers (myosin within cardiomyocytes). All images were 180×180 μm^2 in size (256×256 px^2). To isolate the MP signals from those two regions, a custom software in MATLAB was developed.

For tissue component #1, we operated as follows. From each SHG-TPEF image pair, the algorithm generated the spatial resolved parameter called Index of Aging (INAG) defined as [26]:

$$INAG = \frac{I_{SHG} - I_{TPEF}}{I_{SHG} + I_{TPEF}}, \tag{1}$$

with I_{SHG} and I_{TPEF} being the (point-by-point) intensity of the SHG and TPEF images, respectively. Then, this map was thresholded to create a binary mask of region #1 (BW_{INAG}). This map highlights the SHG signal generated at the interstitial region (at that location this signal is dominant since no TPEF signal was detected). Finally, the product of the original SHG image and the mask provides the final segmented SHG image (SHG_{INTER}) that corresponds exclusively to the interstitial area. This segmentation procedure is based on the method reported by Otsu [46] and uses the local variances of the gray values of the histogram of the INAG image to determine the appropriate threshold before binarization. The flowchart describing the image process to isolate the SHG signal corresponding to the interstitial region is depicted in Fig. 2.

Once SHG_{INTER} is known, the SHG signal density ($SigD$) was computed using Eq. (2):

$$Signal\ Density\ (SigD) = \frac{I_{SHG_{total}}}{N_{PX}}, \tag{2}$$

Biomedical Optics EXPRESS

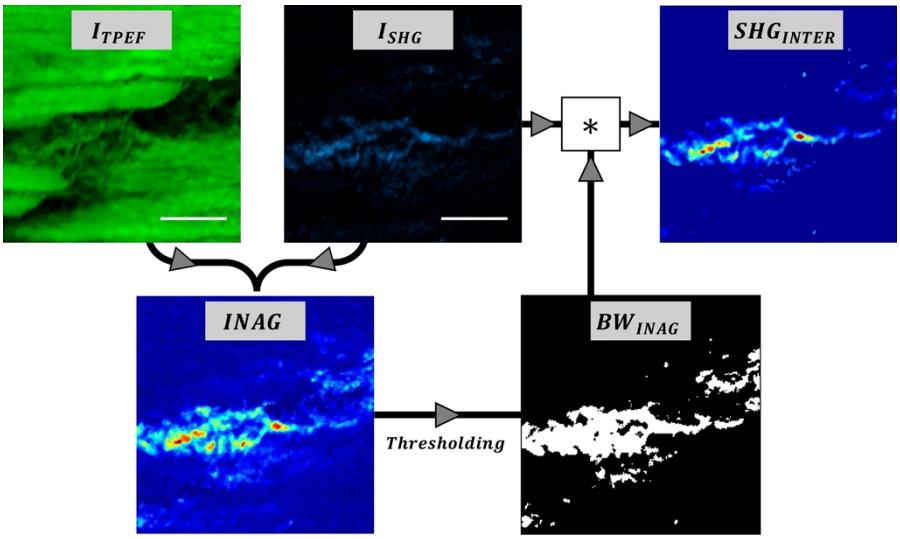

Fig. 2. Image processing workflow to segment the SHG signal from the interstitial region. Scale bars: 50 µm.

where I_{SHG_total} is the total SHG intensity (i.e., the sum of the intensity of each pixel in the segmented image) and N_{PX} is the number of white pixels within the binary mask. Since the size and resolution of the image is known, this value can be expressed in μm^{-2} units. In easy words, *SigD* is a measure of the concentration of the collagen within the imaged tissue. Then, in general terms, the higher *SigD*, the higher the collagen accumulation.

For tissue structure #2, the segmentation of the cardiac muscle fibers was performed in a similar way. First, the TPEF image was thresholded to generate a binary mask (BW_{TPEF}, Fig. 3(a)). This BW_{TPEF} was multiplied by the inverse of mask BW_{INAG} (Fig. 3(b), see Fig. 2 above). The result is another binary mask (BW_{INTRA}, Fig. 3(c)) where the white pixels correspond to the area containing the tissue components #2.

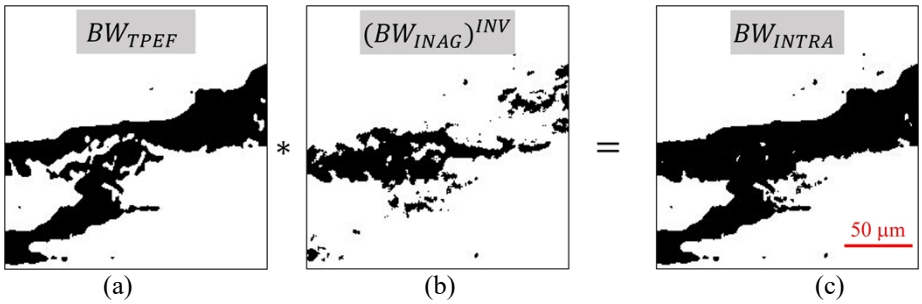

Fig. 3. Procedure to isolate the area occupied by cardiac muscle fibers. The TPEF binary image (BW_{TPEF}, a) is multiplied by the inverse of the binary mask BW_{INTER}, $((BW_{INTER})^{INV}$, b). The result is the mask corresponding to the myocardial fiber segmentation (BW_{INTRA}, c).

Next, the product of the original SHG and TPEF images and the mask BW_{INTRA} provided the final segmented images (SHG_{INTRA} and $TPEF_{INTRA}$) that corresponded exclusively to the cardiac muscle fiber region (Fig. 4). Since this area emits both TPEF and SHG signals [34,35], changes in *SigD* as a function of age can be studied using Eq. (2). Now, in that equation, I_{SHG_total}

Biomedical Optics EXPRESS

(I_{TPEF_total}) represent the total SHG (TPEF) signal of the non-null pixels of the segmented SHG_{INTRA} ($TPEF_{INTRA}$) images, and N_{PX} is the number of white pixels of the new mask BW_{INTRA}.

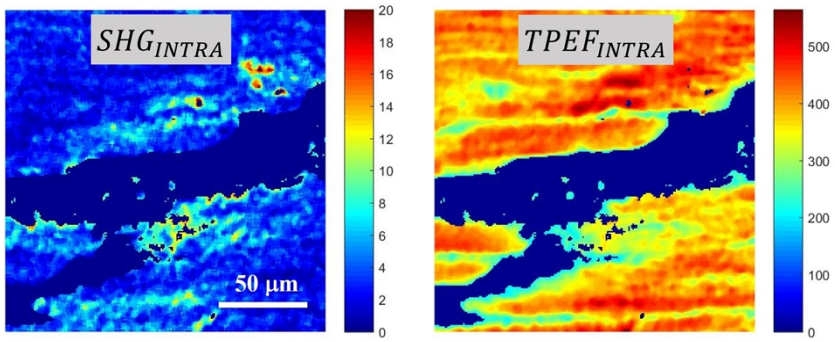

Fig. 4. Representative examples of SHG (a) and TPEF (b) segmented images of the cardiac muscle fiber area.

2.3.2. Collagen organization

The spatial organization of the interstitial collagen fibers appearing in SHG_{INTER} images was quantified by means of the Hough Transform (HT) [47]. HT is a well-established mathematical method able to detect different features within an image, in particular those associated with straight lines. Collagen distribution has been successfully analyzed with this technique in previous works and further details can be found in [48]. The algorithm (also developed in MATLAB) provides a parameter known as the structural dispersion (*SD*). An example of the HT algorithm using an artificial image (composed of horizontal straight lines) is shown in Fig. 5. In brief, the procedure was based on detecting lines within the image (with a certain length pre-defined in the calibration procedure [48]). Each time a new straight line is found, the HT accumulator's bin increments the corresponding value. Green boxes in the HT accumulation matrix (right panel of Fig. 5) indicate the peak of lines found at a distance ρ from the origin at a given orientation, θ_i. As expected, for this image, the value of the angles θ_i detected are around zero. The *SD* of the collagen fibers is defined as the standard deviation of those θ_i. As a general idea, the higher *SD*, the lower the degree of organization of the collagen fibers. In particular, when SD $\leq 20°$ the sample presents a fairly organized structure. This will be non-organized if SD $> 40°$. The range in between corresponds to partially organized arrangements.

Biomedical Optics EXPRESS

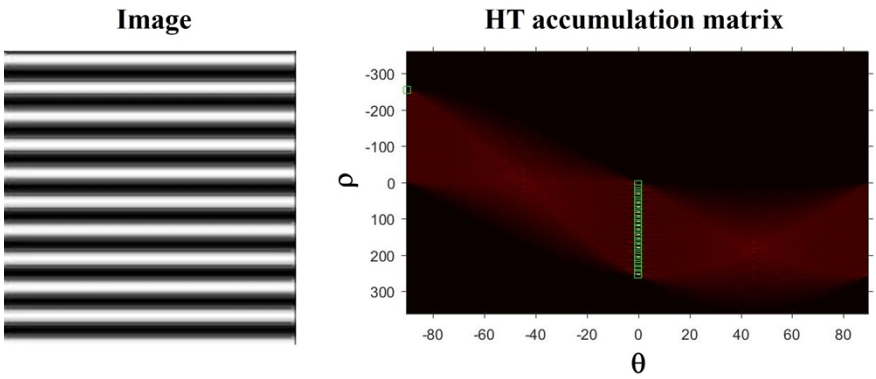

Fig. 5. Example of the use of the HT with an artificial image (left) and the corresponding HT accumulation matrix (right).

3. Results

A representative example of a pair of TPEF and SHG images of a transmural LV section from a young pig is presented in Fig. 6. Instead of individual frames, a 3×3 mosaic of images (one next to each other) was built. This allows the visualization of a bigger area within the tissue. A qualitative observation shows that, whereas SHG signals are generated in both interstitial and cardiac muscle fiber areas, TPEF signals can only be seen in the latter. For these images the average TPEF signal (501 ± 39 a.u.) was 16 times higher than that of SHG signal (38 ± 21 a.u.).

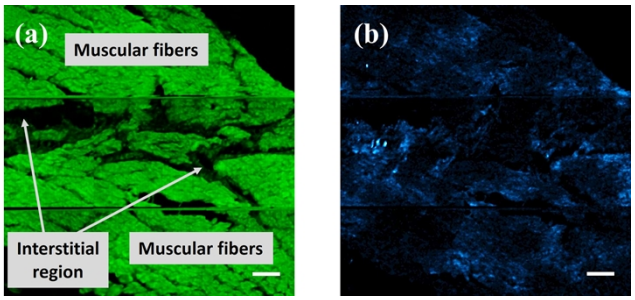

(a) (b)

Fig. 6. TPEF (a) and SHG (b) images (3×3 mosaic, 540×540 µm^2) of a non-stained young pig transmural LV tissue section. For a direct comparison, both images share the same color scale. Labels have been included in Fig. 6(a) for a better identification of the two regions of interest. Bar length: 50 µm.

SHG signal in the interstitial area is generated by the collagen fibers there located [34,39,43]. In the cardiac muscle fiber region, both MP signals are produced: whereas SHG arises from the myosin lattice of muscle cells [14], TPEF signal might come from different cardiomyocyte autofluorescent cellular components (mostly proteins) [33]. The choice of the spectral filters used in our experimental system avoids contamination of TPEF signals in the SHG channel. Then, SHG signal from the cardiac muscle fiber is associated to pure myosin signal.

Biomedical Optics EXPRESS

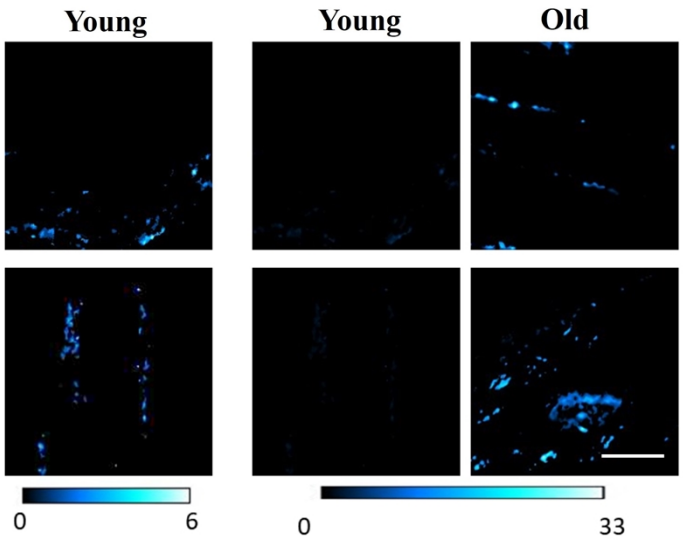

Fig. 7. SHG images from the isolated interstitial region with collagen content. Left and middle panels: young specimens presented using different color scales (as indicated with the bars at the bottom). Right panels: old specimens. Scale bar: 50 µm.

3.1. Changes in the interstitial region

3.1.1. Interstitial collagen concentration

SHG images of the interstitial region were obtained using the procedure explained in the Methods section. As described above, the cardiac interfibrillar areas with collagen content were isolated. Representative SHG images for two samples from each age group are presented in Fig. 7.

Panels in central and right columns correspond to young and old specimens, respectively. However, since the SHG signal in the former is noticeable lower than in the latter, when both are represented using the same color scale, collagen features are not visible in samples from young animal models (see middle panels and color bars in Fig. 7). Left panel are the same than those in the central column but presented with a different color scale (in order to observe biological details).

Once all the SHG images were segmented, *SigD* corresponding to interstitial collagen was computed. Averaged values for both age groups are shown in Fig. 8. As expected from the previous figure, an increment in the interstitial collagen density of ~3.6x was found when comparing young and old samples. Although old samples present a higher variance, differences with age were statistically significant ($p < 0.001$, Welch's t test).

3.1.2. Interstitial collagen organization

An objective analysis of the interstitial collagen arrangement was also carried out by means of the HT algorithm (see section 2.3.2). This allows quantifying its degree of organization as depicted in Fig. 9. The plot depicts the averaged *SD* values for both groups of age. A noticeable higher collagen organization level (i.e., lower *SD*) was found for old specimens (~2-fold). The statistical analysis shows significant differences among the two sets of specimens ($p < 0.001$, Welch's t test).

For the sense of completeness, Fig. 10 presents two illustrative examples of the results obtained using the HT in a young and an old heart sample. Green boxes in the accumulation matrices (right panels) indicate the orientations corresponding to the segments marked in the SHG images (left panels). For the old sample it can be observed that the segments (i.e. collagen fibers) are

Biomedical Optics EXPRESS

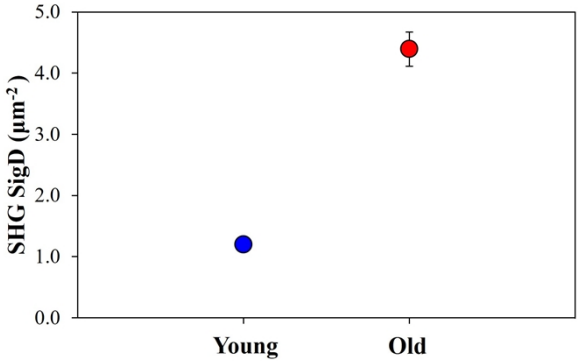

Fig. 8. Interstitial collagen *SigD* values for young (blue) and old (red) samples for the interstitial tissue component Each symbol represents the value averaged across all specimens and imaged areas. Error bars are the standard deviation (the error bar for the young samples is smaller than the blue symbol).

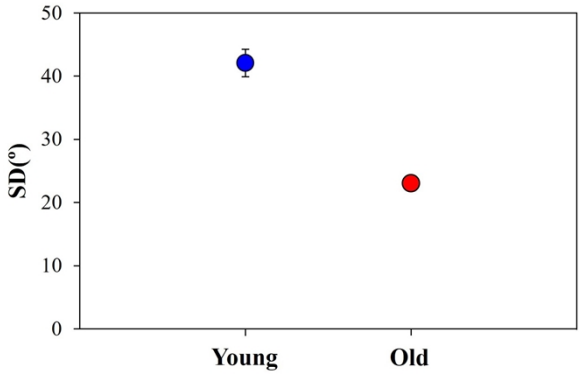

Fig. 9. SD values of the interstitial collagen organization for young and old samples. Each symbol and bar represent the same as in Fig. 8.

mainly lying along a preferential orientation. This leads to a *SD* value of 21°, what is associated with a fairly organized structure [48]. On the opposite, for the young specimen these fibers are not that well organized, and the value of *SD* (42°) corresponds to a non-organized structure.

3.2. Changes in the cardiac muscle fibers

Figure 11 shows SHG images of the cardiac muscle fibers from a young and an old pig heart. These images are a result of the procedure described above, which is able to isolate that tissue component through the use of the BW_{INTRA} mask. As stated above, this SHG signal arises from the myosin located within the cardiomyocytes. Images are represented with the same signal intensity scale for direct comparisons. A direct observation reveals noticeable differences in the SHG intensity between both images. In particular, the SHG signal was ~3.5 times higher in the old specimen compared to the young one. A similar behavior was found for the corresponding TPEF images.

To explore in detail the differences between the two sets of samples involved in the present study, Fig. 12 depicts the intracellular *SigD* values as a function of age for both MP signals. Each symbol represents the value averaged across all specimens and imaged areas. SHG experimental data show a statistically significant difference between both age groups ($p < 0.001$,

Biomedical Optics EXPRESS

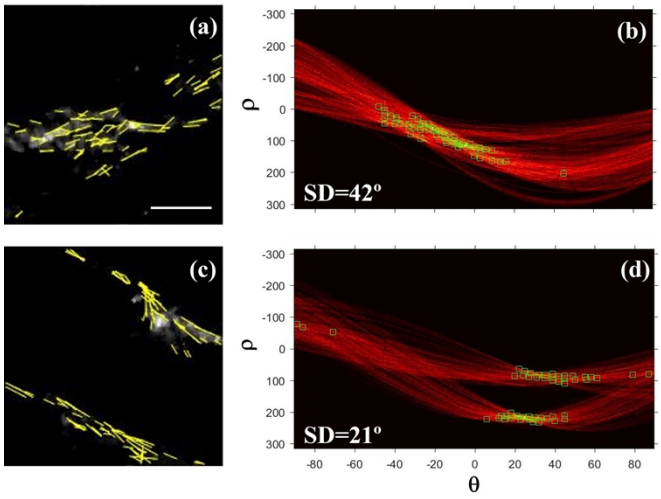

Fig. 10. SHG images of the interstitial collagen in a young (a) and an old sample (c). Overlapped yellow lines represent the lines detected by the HT algorithm. (b, d) Corresponding HT accumulation matrices for both images. Green boxes indicate the orientation of the lines detected within the images. Bar length: 50 µm.

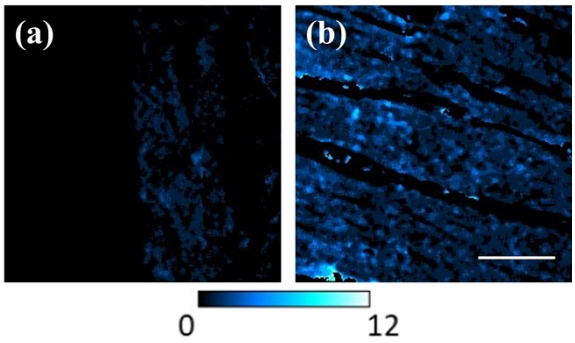

Fig. 11. SHG images of the cardiac muscle region in a young (a) and old (b) sample. For visual comparisons, both images are presented with the same the color scale bar scale (see inset). Scale bar: 50 µm.

Mann-Whitney U). TPEF *SigD* also differed significantly between young and old specimens ($p < 0.001$, Mann-Whitney U).

Biomedical Optics EXPRESS

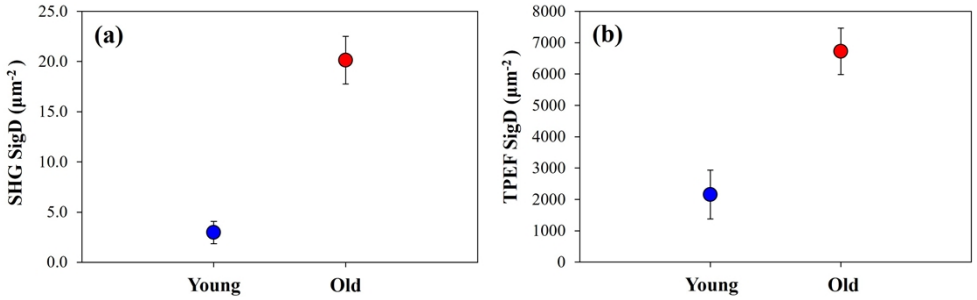

Fig. 12. Averaged values of SigD for SHG (a) and TPEF (b) signals in young and old samples for the cardiac fiber tissue component. Error bars: standard error of the mean. The labels are the same as in previous figures.

4. Discussion and conclusions

Treating and preventing heart disease is a major societal and health challenge. Aging emphasizes cardiac problems and better ways to manage CVD are urgently required. Imaging technologies are helping to analyze morphological changes in cardiac tissues. These include near-infrared spectroscopy, optical coherence tomography and fluorescent lifetime procedures, among others [49]. MP imaging procedures have been shown to be useful in imaging very different types of tissues, both healthy and pathological [15,18–25]. In particular, this method has also been employed to extract qualitative structural information from cardiomyocytes [34–36]. Moreover, the combination of TPEF and SHG signals has proved to be a useful tool to evaluate age-related changes in tissues from different organs in a label free manner [26,27,29].

As cardiac tissue ages, a variety of alterations occur [50]. Whereas some are related to normal physiological age-related changes, others are associated with disease. In the process of getting old, cardiac tissues suffer from abundant interstitial fibrosis, a process that involves excess deposition of collagen type I [3]. This fibrosis impairs cardiac muscle relaxation and may result in heart failure. LV collagen deposition was reported to be higher in elderly individuals than in young individuals [3,5,51]. This increase in the degree of LV fibrosis was also shown to lead to ventricular dysfunction [52]. Apart from the collagen amount, its arrangement and spatial distribution play a role in cardiac function [53]. In addition to myocardial collagen content increase, evidence of aging-related cardiomyocyte alterations has been reported [2]. Cardiac growth and structural maturation in aged hearts also exhibit cardiomyocyte senescence even in the absence of underlying pathology [2,49].

Therefore, it is crucial to improve existing methods by developing alternative tools to conduct more reliable assessment of cardiac age-related changes. TPEF images were subtracted from SHG images to differentiate control and diseased hearts following hypertrophic remodeling [40]. Since interstitial collagen and intracellular myosin are strong SHG emitters [34,39,43], and TPEF signal is only produced by cardiomyocytes [33], herein we have proposed a procedure based on the combination of SHG-TPEF image pairs to objectively assess differences in cardiac remodeling, applied to the study of the effect of age in LV tissues. The approach is able to accurately segment interstitial and cardiac muscle areas and compute the density of both MP signals independently.

In the present study, interstitial collagen SHG signal in old specimens was on average 3.8x larger than that corresponding to young ones. Interestingly, the SHG signal can also be analyzed to extract quantitative information on collagen spatial arrangement. The algorithm uses the HT to automatically identify collagen fibers and assess their organization (as measured with the parameter SD) [48]. Young LV tissues were found to exhibit a non-regular distribution of

Biomedical Optics EXPRESS

interstitial collagen fibers. In terms of SD, the values in young specimens were mostly above 40°, indicating the absence of a preferential orientation. On the opposite, the values in old tissues were around 20°, what represent high-organized collagen arrangements.

The developed method allows to extract novel information regarding collagen and myosin features during cardiac aging beyond the currently described ones relative to amount and spatial distribution [6]. In addition to the known increase in collagen content with age, our current data indicate that collagen density also increases. Since collagen is a main structural component of the extracellular matrix, the density increase probably leads to more compact bundles, which may lead to changes in the physical properties of the myocardium, e.g. reducing its elasticity. This agrees with the well-known increase in LV wall stiffness occurring in elderly hearts, both in animal models and humans [2,3]. Also, the increased organization with age aligns with the expected effect of the increase in collagen density. The result of the spatial conformational changes in the collagen fibers gaining directionality could led to increased strength of the collagen bundles, and thus higher LV wall stiffness.

Results for myosin reveal that SHG signal density is significantly higher in cardiac tissue samples from old versus young pigs (>6-fold on average). For cardiomyocyte TPEF signal, differences between young and old tissue specimens, were smaller (~3x) but still statistically significant. This would suggest a remodeling of the myosin compartment with age, which could have an effect on the LV functionality given the main role of MYH6/7 in cardiac contraction, especially in relation to the well-known age-related diastolic dysfunction [2]. Whether the variations in the SHG signal are due to an altered balance of MYH6/7 or the structural arrangement of these sarcomeric proteins requires further investigation.

This study is a proof-of-concept to demonstrate the reliability of the method to extract quantitative differences in porcine heart tissues having extreme young and old phenotypes. The number of samples used is reduced, however, our goal was not to characterize the effects of age on cardiac tissue but to develop a useful procedure to objectively analyze myosin concentration and structural arrangements of interstitial collagen through the analysis of TPEF and SHG signals in cardiac tissue.

In conclusion, here we acquire biological data in a label free fashion and develop a method to quantify novel features related to cardiac remodeling. This is a proof-of-concept study to demonstrate the utility of the developed methodology to underscore phenotypic changes present with age in a limited number of pig LV samples. Further characterization of the age-related cardiac remodeling in this model system of the human LV [5] would require a larger number of specimens. Of note, the reported procedure can be applied to study other cardiac pathologies related to collagen and sarcomeric alterations.

Funding. Agencia Estatal de Investigación (PID2019-105674RB-I00, PID2020-113919RB-I00/AEI/10.13039/501100011033, PID2022-139859OB-I00, PID2022-140556OB-I00, TED2021-130459B-I00).

Disclosures. The authors declare no conflicts of interest and have no proprietary interest in any of the materials mentioned in this article.

Data availability. Data underlying the results presented in this paper are not publicly available at this time but may be obtained from the authors upon reasonable request.

References

1. World Health Organisation. Cardiovascular Diseases (2021).
2. A. Biernacka and N. G. Frangogiannis, "Aging and cardiac fibrosis," Aging Dis. **2**(2), 158–173 (2011).
3. M. A. Horn and A. W. Trafford, "Aging and the cardiac collagen matrix: Novel mediators of fibrotic remodelling," J. Mol. Cell. Cardiol. **93**, 175–185 (2016).
4. S. Rozenberg, B. Tavernier, B. Riou, *et al.*, "Severe impairment of ventricular compliance accounts for advanced age-associated hemodynamic dysfunction in rats," Exp. Gerontol. **41**(3), 289–295 (2006).
5. E. Ramos-Marquès, L. García-Mendívil, M. Pérez-Zabalza, *et al.*, "Chronological and biological aging of the human left ventricular myocardium: Analysis of microRNAs contribution," Aging Cell **20**(7), e13383 (2021).
6. L. García-Mendívil, M. Pérez-Zabalza, K. Mountris, *et al.*, "Analysis of age-related left ventricular collagen remodeling in living donors: implications in arrhythmogenesis," iScience **25**(2), 103822 (2022).

Biomedical Optics EXPRESS

7. M. P. Guota, "Factors controlling cardiac myosin-isoform shift during hypertrophy and heart failure," J. Mol. Cell. Cardiol. **43**(4), 388–403 (2007).
8. T. J. Herron and K. S. McDonald, "Small amounts of α-myosin heavy chain isoform expression significantly increase power output of rat cardiac myocyte fragments," Circ. Res. **90**(11), 1150–1152 (2002).
9. M. R. Locher, M. V. Razumova, J. E. Stelzer, *et al.*, "Effects of low-level α-myosin heavy chain expression on contractile kinetics in porcine myocardium," Am. J. Physiol. Heart Circ. Physiol. **300**(3), H869–H878 (2011).
10. S. Miyata, W. Minobe, M. R. Bristow, *et al.*, "Myosin Heavy Chain Isoform Expression in the Failing and Nonfailing Human Heart," Circ. Res. **86**(4), 386 (2000).
11. B. D. Lowes, W. Minobe, W. T. Abraham, *et al.*, "Changes in gene expression in the intact human heart. Downregulation of alpha-myosin heavy chain in hypertrophied, failing ventricular myocardium," J. Clin. Invest. **100**(9), 2315–2324 (1997).
12. W. R. Zipfel, R. M. Williams, and W. W. Webb, "Nonlinear magic: Multiphoton microscopy in the biosciences," Nat. Biotechnol. **21**(11), 1369–1377 (2003).
13. R. M. Williams, W. R. Zipfel, and W. W. Webb, "Interpreting second-harmonic generation images of collagen I fibrils," Biophys. J. **88**(2), 1377–1386 (2005).
14. S. V. Plotnikov, A. C. Millard, P. J. Campagnola, *et al.*, "Characterization of the myosin-based source for second-harmonic generation from muscle sarcomeres," Biophys. J. **90**(2), 693–703 (2006).
15. F. Helmchen and W. Denk, "Deep tissue two-photon microscopy," Nat. Methods **2**(12), 932–940 (2005).
16. R. LaComb, O. Nadiarnykh, S. S. Townsend, *et al.*, "Phase matching considerations in second harmonic generation from tissues: Effects on emission directionality, conversion efficiency and observed morphology," Opt. Comm. **281**(7), 1823–1832 (2008).
17. O. del Barco and J. M. Bueno, "Second harmonic generation signal in collagen fibers: role of polarization, numerical aperture, and wavelength," J. Biomed. Opt. **17**(4), 045005 (2012).
18. P. J. Campagnola and C.-Y. Dong, "Second harmonic generation microscopy: principles and applications to disease diagnosis," Laser Photonics Rev. **5**(1), 13–26 (2011).
19. M.-H. Chen, W.-L. Chen, Y. Sun, *et al.*, "Multiphoton autofluorescence and second-harmonic generation imaging of the tooth," J. Biomed. Opt. **12**(6), 064018 (2007).
20. C. Rodríguez and N. Ji, "Adaptive optical microscopy for neurobiology," Curr. Opin. Neurobiol. **50**, 83–91 (2018).
21. J. M. Bueno, Y.-S. Liao, F. J. Ávila, *et al.*, "Drosophila brain advanced multiphoton imaging," in *Advances in Brain Imaging Techniques*, N. Mazumder, G. Gangadharan, and Y. V. Kistenev, eds. (Springer, 2022).
22. A. Keikhosravi, J. S. Bredfeldt, A. K. Sagar, *et al.*, "Second-harmonic generation imaging of cancer," Methods Cell Biol. **123**, 531–546 (2014).
23. S.-J. Lin, S.-H. Jee, C.-J. Kuo, *et al.*, "Discrimination of basal cell carcinoma from normal dermal stroma by quantitative multiphoton imaging," Opt. Lett. **31**(18), 2756–2758 (2006).
24. F. J. Ávila, P. Artal, and J. M. Bueno, "Quantitative discrimination of healthy and diseased corneas with second harmonic generation microscopy," Trans. Vis. Sci. Tech. **8**(3), 51 (2019).
25. A. Batista, H. G. Breunig, A. König, *et al.*, "High-resolution, label-free two-photon imaging of diseased human corneas," J. Biomed. Opt. **23**(3), 036002 (2018).
26. S.-J. Lin, R. Wu, H.-Y. Tan, *et al.*, "Evaluating cutaneous photoaging by use of multiphoton fluorescence and second harmonic," Opt. Lett. **30**(17), 2275–2277 (2005).
27. M. Koehler, K. König, P. Elsner, *et al.*, "In vivo assessment of human skin aging by multiphoton laser scanning tomography," Opt. Lett. **31**(19), 2879–2882 (2006).
28. D. Aït-Belkacem, M. Guilbert, M. Roche, *et al.*, "Microscopic structural study of collagen aging in isolated fibrils using polarized second harmonic generation," J. Biomed. Opt. **17**(8), 080506 (2012).
29. J. M. Bueno, R. M. Martínez-Ojeda, A. C. Fernández-Escudero, *et al.*, "Dental age estimation using multiphoton microscopy: A potential tool for forensic science," BioMed Res. Int. **2022**, 3328818 (2022).
30. M. Rubart, E. Wang, K. W. Dunn, *et al.*, "Two-photon molecular excitation imaging of Ca2 + transients in Langendorff-perfused mouse hearts," Am. J. Physiol. Cell Physiol. **284**(6), C1654–C1668 (2003).
31. M. Rubart, K. B. Pasumarthi, H. Nakajima, *et al.*, "Physiological coupling of donor and host cardiomyocytes after cellular transplantation," Circ. Res. **92**(11), 1217–1224 (2003).
32. M. Rubart, M. H. Soonpaa, H. Nakajima, *et al.*, "Spontaneous and evoked intracellular calcium transients in donor-derived myocytes following intracardiac myoblast transplantation," J. Clin. Invest. **114**(6), 775–783 (2004).
33. J. A. Scherschel and M. Rubart, "Cardiovascular imaging using two-photon microscopy," Microsc. Microanal. **14**(6), 492–506 (2008).
34. W. R. Zipfel, R. M. Williams, R. Christie, *et al.*, "Live tissue intrinsic emission microscopy using multiphoton-excited native fluorescence and second harmonic generation," Proc. Natl. Acad. Sci. U. S. A **100**(12), 7075–7080 (2003).
35. S. J. Wallace, J. L. Morrison, K. J. Botting, *et al.*, "Second harmonic generation and two-photon-excited autofluorescence microscopy of cardiomyocytes: quantification of cell volume and myosin filaments," J. Biomed. Opt. **13**(6), 064018 (2008).
36. T. Boulesteix, E. Beaurepaire, M. P. Sauviat, *et al.*, "Second-harmonic microscopy of unstained living cardiac myocytes: measurements of sarcomere length with 20-nm accuracy," Opt. Lett. **29**(17), 2031–2033 (2004).
37. A. Zoumi, X. Lu, G. S. Kassab, *et al.*, "Imaging coronary artery microstructure using second harmonic and two-photon fluorescence microscopy," Biophys. J. **87**(4), 2778–2786 (2004).

Biomedical Optics EXPRESS

38. K. Schenke-Layland, I. Riemann, U. A. Stock, *et al.*, "Imaging of cardiovascular structures using near-infrared femtosecond multiphoton laser scanning microscopy," J. Biomed. Opt. **10**(2), 024017 (2005).
39. M. R. Tsai, Y. W. Chiu, M. T. Lo, *et al.*, "Second-harmonic generation imaging of collagen fibers in myocardium for atrial fibrillation diagnosis," J. Biomed. Opt. **15**(2), 026002 (2010).
40. T. P. Martin, G. Norris, G. McConnell, *et al.*, "A novel approach for assessing cardiac fibrosis using label-free second harmonic generation," Int. J. Cardiovasc. Imaging **29**(8), 1733–1740 (2013).
41. J. D. Nicolas, A. Khan, A. Markus, *et al.*, "X-ray diffraction and second harmonic imaging reveal new insights into structural alterations caused by pressure-overload in murine hearts," Sci. Rep. **10**(1), 19317 (2020).
42. J. Pichon, M. Ledevin, T. Larcher, *et al.*, "Label-free 3D characterization of cardiac fibrosis in muscular dystrophy using SHG imaging of cleared tissue," Biol. Cell **114**(3), 91–103 (2022).
43. A. Khan, F. Ramos-Gomes, A. Markus, *et al.*, "Label-free imaging of age-related cardiac structural changes in non-human primates using multiphoton nonlinear microscopy," Biomed. Opt. Express **12**(11), 7009–7023 (2021).
44. A. Oliván-Viguera, M. Pérez-Zabalza, L. García-Mendívil, *et al.*, "Minimally invasive system to reliably characterize ventricular electrophysiology from living donors," Sci. Rep. **10**(1), 19941 (2020).
45. J. M. Bueno, A. Giakoumaki, E. J. Gualda, *et al.*, "Analysis of the chicken retina with an adaptive optics multiphoton microscope," Biomed. Opt. Express **2**(6), 1637–1648 (2011).
46. N. Otsu, "A threshold selection method from gray level histograms," IEEE Trans. Syst., Man, Cybern. **9**(1), 62–66 (1979).
47. A. Herout, M. Dubská, and J. Havel, "Review of Hough transform for line detection," in *Real-Time Detection of Lines and Grids*, (Springer, 2013).
48. J. M. Bueno, F. J. Ávila, R. Hristu, *et al.*, "Objective analysis of collagen organization in thyroid nodule capsules using second harmonic generation microscopy images and the Hough transform," Appl. Opt. **59**(23), 6925–6931 (2020).
49. L. Marcu, "Photonics improves interventional cardiology," BioPhotonics, May/June 2023, pg. 7.
50. V. Obas and R. S. Vasan, "The aging heart," Clin. Sci. **132**(13), 1367–1382 (2018).
51. C. R. Gazoti Debessa, L. B. Mesiano Maifrino, and R. Rodrigues de Souza, "Age related changes of the collagen network of the human heart," Mech. Ageing Dev. **122**(10), 1049–1058 (2001).
52. A. B. L. Mendes, M. Ferro, B. Rodrigues, *et al.*, "Quantification of left ventricular myocardial collagen system in children, young adults, and the elderly," Medicina **72**(3), 216–220 (2012).
53. A. González, E. B. Schelbert, J. Díez, *et al.*, "Myocardial interstitial fibrosis in heart failure: Biological and translational perspectives," J. Am. Coll. Cardiol. **71**(15), 1696–1706 (2018).